

**Extreme events in systems with discontinuous boundaries**

Suresh Kumarasamy

*Department of Physics and Astrophysics, University of Delhi, Delhi 110007, India*

Alexander N. Pisarchik

*Center for Biomedical Technology, Technical University of Madrid, Campus Montegancedo, Pozuelo de Alarcón, 28223 Madrid, Spain*

(Received 13 April 2018; published 4 September 2018)

We describe a class of extreme events emerging in systems with discontinuous boundaries that exhibit stick-slip dynamics. This kind of systems is capable of generating extreme events when the system trajectory sticks to a sliding set and slides for a relatively large distance along the discontinuous boundary to one of the system's subspaces. We present two examples of such systems, a microelectromechanical cantilever and a driven class-B laser, where this type of extreme events appear. We show that their forecasting is possible by monitoring the sliding trajectory along the discontinuous boundary. In both cases, the probability distribution of recurrence times exhibits a power-law behavior, typical for extreme events. The results of this study can be of interest for engineering applications, for example, to predict extremely large-amplitude oscillations in cantilevers, systems with friction, lasers, and other systems with discontinuous boundaries.

DOI: [10.1103/PhysRevE.98.032203](https://doi.org/10.1103/PhysRevE.98.032203)**I. INTRODUCTION**

Extreme events are rare unexpected events suddenly occurring in nature, engineering, and social life. Examples of such events are rogue waves, cyclones, tsunamis, floods, droughts, earthquakes, finance pandemics, influenza, power outages, material ruptures, explosions, chemical contamination, etc. [1–4]. Even though the emergence of extreme events is not likely, they can produce enormous destruction and economic losses. Therefore, many researchers from different areas of science have been focusing in studying the mechanisms underlying such events in order to anticipate their appearance.

Though there is no strict mathematical definition of extreme events, it is largely accepted that they imply a heavily tailed probability distribution and at least four times the standard deviation over peaks' average. Using the above criteria, the extreme events have been identified in linear [5–9] and nonlinear [10–19] dynamical systems, modeled by partial and ordinary differential equations and observed in superfluid helium [5], plasma [7], optical fibers [6,15], lasers [16,17,20], forced Liénard system [19], gravity and capillary waves [21], etc. The experimental evidence of extreme events has also been demonstrated in many scientific laboratories [5–8,10,16,17,19–22].

The underlying mechanisms of extreme events were shown to have either stochastic or deterministic nature. While in noisy systems, extreme events can arise due to multistability [16] or noise-induced transitions far from equilibrium [23], in pure deterministic systems, they can appear due to nonlinearity and chaos [17,20,24–26]. Despite extensive studies of extreme events, their origin in many dynamical systems remains unknown. The classical theory of extreme values says that they can obey various statistical distributions, such as Fréchet, Gumbel, Weibull, etc., depending on the

probability density tail [27]. Although there are no universal rules for all existing extreme events, we may expect that some classes of extreme events obey specific laws. The discovery of common properties inherent to a certain class of extreme events remains a challenge for nonlinear dynamics.

In this paper, we introduce a new class of extreme events which emerges in dissipative systems with discontinuous boundaries. Such systems are frequently encountered in many fields of science and engineering, from the cantilever bridge over the Rhine River between Germany and France to complex electronic and optical devices. The examples include systems with friction [28], micro-electro-mechanical system (MEMS) cantilevers [29], class-B lasers [24,30,31], the Olsen model for the peroxidase-oxidase reaction [32], mass-spring-damper oscillator [33], etc. The existence of a sliding portion along the discontinuous boundary is a specific feature of these systems. The basic concept of systems with discontinuous boundaries was developed by Filippov [34]. Since then, many scientists have used and extend the Filippov's theory to investigate dynamics of such systems [33,35–38].

The sliding motion is a constrained evolution of the trajectory in a subset of the system's state space. The transition between orbits with and without sliding portions occurs in a discontinuous bifurcation [35], also known as a *sliding bifurcation* [36]. This bifurcation, typical in nonlinear systems with discontinuous vector fields, can occur due to a piecewise function, discontinuity in equations, singularity, or boundary conditions. It is worth noting that the sliding bifurcation through stick-slip motion was also studied in the context of earthquakes [39] which emergence was referred to self-organized criticality [40]. However, the mechanism behind the extreme events in the systems with discontinuous boundaries and the stick-slip bifurcation is not yet well understood.

Here we consider two paradigmatic examples of systems with discontinuous boundaries, namely, a cantilever-based

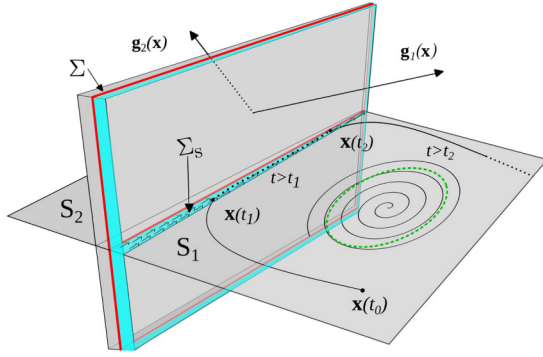


FIG. 1. Schematic representation of a system with a discontinuous boundary.

MEMS and a modulated CO<sub>2</sub> laser, both having discontinuous boundaries, the former because of singularity, while the latter due to boundary conditions. We demonstrate that near a stick-slip bifurcation, the system trajectory sticks and slides along the discontinuous boundary, and after slipping away from the boundary, it makes a long excursion that results in a large-amplitude oscillation. However, this bifurcation never occurs when the trajectory is far away from the discontinuous boundary; it only appears when the trajectory approaches the boundary.

The paper is organized as follows. In Sec. II we describe the system with a discontinuous boundary in a general form. Then, in Secs. III and IV we consider particular examples of systems with discontinuous boundaries, namely, the MEMS and laser models. Finally, in Sec. V we summarize our results.

## II. DYNAMICAL SYSTEMS WITH DISCONTINUOUS BOUNDARIES

In general, a system with a discontinuous boundary (Fig. 1) can be written in the vector form as follows:

$$\dot{\mathbf{x}} = \begin{cases} \mathbf{g}_1(\mathbf{x}), & \mathbf{x} \in S_1 \\ \mathbf{g}_2(\mathbf{x}), & \mathbf{x} \in S_2 \end{cases}, \quad (1)$$

where  $\dot{\mathbf{x}}$  is the time derivative of vector variable  $\mathbf{x}$  and  $\mathbf{g}_1$  and  $\mathbf{g}_2$  are vector fields in subspaces  $S_1$  and  $S_2$ , respectively, separated by discontinuous boundary  $\Sigma = \{\mathbf{x} \in \mathbf{R}^2 : H(\mathbf{x}) = 0\}$ , where  $H(\mathbf{x})$  represents a nonvanishing smooth scalar gradient function on  $\Sigma$ , such that  $S_1 = \{\mathbf{x} \in \mathbf{R}^2 : H(\mathbf{x}) < 0\}$  and  $S_2 = \{\mathbf{x} \in \mathbf{R}^2 : H(\mathbf{x}) > 0\}$ .

The discontinuous boundary  $\Sigma$  can be either infinite in the presence of singularity or closed in the presence of a boundary equilibrium point. The inequality  $\mathbf{g}_1 \neq \mathbf{g}_2$  takes place in all points on  $\Sigma$ . There is a point in the sliding set  $\Sigma_S = \{x \in \Sigma : \sigma(x) \leq 0\}$  [ $\sigma(x) = \langle H_x(x), \mathbf{g}_1(x) \rangle \langle H_x(x), \mathbf{g}_2(x) \rangle$ ], where the vector fields  $\mathbf{g}_1$  and  $\mathbf{g}_2$  are tangent to  $\Sigma$  [41].

The system trajectory starting at initial condition  $\mathbf{x}(0)$  in region  $S_1$  is attracted to a unique solution  $\mathbf{x}(t)$ . If the trajectory is far away from  $\Sigma_S$ , then the solution of Eq. (1) is either a stable limit cycle or a fixed point. The trajectory  $\mathbf{x}(t)$  reaches the sliding set  $\Sigma_S$  at the moment  $t_1$  and leaves it at  $t_2$ . Thus, the sliding trajectory flows along  $\Sigma_S$  from point  $\mathbf{x}(t_1)$  to point  $\mathbf{x}(t_2)$  ( $t_2 > t_1$ ), passing the sliding distance  $\mathbf{x}_{sd} = \mathbf{x}(t_2) - \mathbf{x}(t_1)$ .

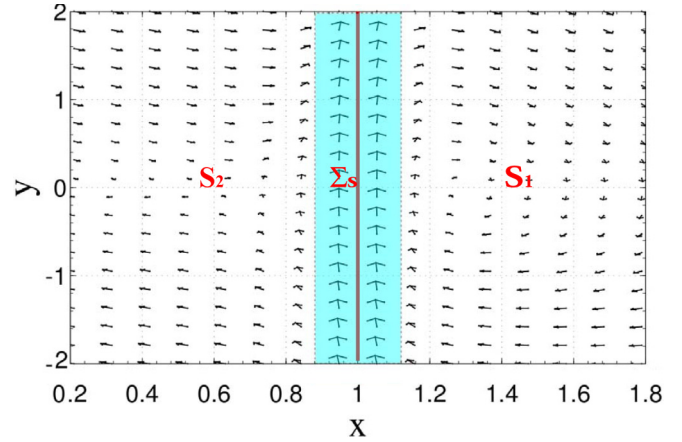


FIG. 2. MEMS vector field near the discontinuous boundary at  $x = 1$ .

Due to the discontinuity, there is a boundary equilibrium tangent point, so that the trajectory begins to recede from the sliding set  $\Sigma_S$  at point  $\mathbf{x}(t_2)$ , making a long excursion and remaining in  $S_1$  for the entire time  $t > t_2$ , never entering  $S_2$ .

## III. SLIDING BIFURCATION AND EXTREME EVENTS IN MEMS CANTILEVERS

To elucidate how the discontinuity-induced bifurcation leads to extreme events, let us consider first a MEMS cantilever consisting of a nonlinear mass-spring-damper system with external electrostatic action. It is worth mentioning that MEMS technology is widely used in miniaturized structures, such as microelectronics, microsensors, and microactuators. It conveys the advantages of miniaturization of multiple components to design integrated electromechanical systems and microsensors for almost every possible sensing modality, including pressure, radiation, temperature, inertial force, magnetic field, chemical species, etc. [42].

### A. MEMS model

The dimensionless MEMS model is given as [29]

$$\dot{x} = y, \quad \dot{y} = -\gamma y - x + \frac{\beta^2}{(1-x)^2} + \alpha \cos(\omega t), \quad (2)$$

where variables  $x$  and  $y$  are related to the displacement and electrostatic voltage, respectively, and  $\alpha$  and  $\omega$  are the amplitude and frequency of an external disturbance. The system Eq. (2) has a discontinuous boundary  $\Sigma$  due to the presence of singularity at  $x = 1$ . Therefore, the system has two subspaces  $S_1$  and  $S_2$  at  $x > 1$  and  $x < 1$ , respectively.

In Fig. 2 we plot the vector field of the MEMS cantilever in the absence of external perturbation, i.e., for  $\alpha = 0$ . The red vertical line at  $x = 1$  indicates the discontinuous boundary  $\Sigma$ . The shaded regime in aqua color shows the sliding set  $\Sigma_S$ , where the vector field of MEMS is tangent to the discontinuous boundary. When the trajectory enters into any point of this sliding set  $\Sigma_S$ , it slides for a longer distance near the discontinuous boundary  $\Sigma$ .

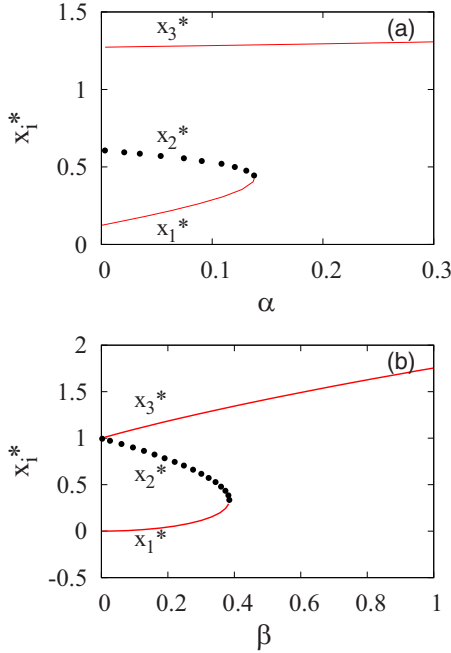


FIG. 3. Stability of fixed point  $x_i^*$  ( $i = 1, 2, 3$ ) as a function of (a)  $\alpha$  for  $\beta = 0.318$  and (b)  $\beta$  for  $\alpha = 7.99$ .

**B. Stability analysis**

Due to nonlinearity in the electrostatic action, the MEMS cantilever can be unstable. With parameters  $\gamma = 0.709$  and  $\beta = 0.318$  without external forcing ( $\alpha = 0$ ), the system Eq. (2) has three fixed points (two stable and one unstable), whereas in the presence of external perturbation with  $\omega = 1.28$  and  $\alpha > 0.138$ , there is only one equilibrium point (stable focus) at  $x > 1$ . Figure 3 shows the positions of these fixed points with respect to the control parameters  $\alpha$  and  $\beta$ . From Fig. 3(a) one can see that when the amplitude  $\alpha$  of the external forcing increases, the equilibrium points  $x_1^*$  and  $x_2^*$  collide at  $\alpha = 0.138$ , so that beyond this amplitude only one stable equilibrium remains.

Figure 3(b) shows that when  $\beta = 0$  the system has one stable equilibrium point at (0,0) and has no sliding orbit or discontinuous boundary. However, when  $\beta > 0$  the sliding orbit arises in the sliding bifurcation. In the range  $0 < \beta < 0.38$ , three equilibrium points coexist and beyond  $\beta > 0.38$  the equilibrium points  $x_1^*$  and  $x_2^*$  collide and disappear, so that only one stable equilibrium point remains. Thus, for the chosen parameters  $\alpha = 7.99$ ,  $\gamma = 0.709$ ,  $\beta = 0.318$ , and  $\omega = 1.28$  the trajectories started in the subspace  $S_1$  always remain in it. When the trajectory approaches the discontinuous boundary at  $x = 1$ , it sticks to the sliding set, slides for a large distance and slips for a long excursion in the subspace  $S_1$ .

**C. Extreme events in MEMS**

For definition, we consider the displacement of  $x$  as an extreme event, when it exceeds 4 times the standard deviations  $\sigma_x$  over average peak amplitude  $\langle x \rangle$ , i.e., the extreme event amplitude is defined as  $x_{EE} = \langle x \rangle + n\sigma_x$ , when  $n \geq 4$ . We find that MEMS satisfies this criterion when the modulation amplitude  $\alpha$  exceeds a threshold value  $\alpha_{th} = 7.7$ . In the right

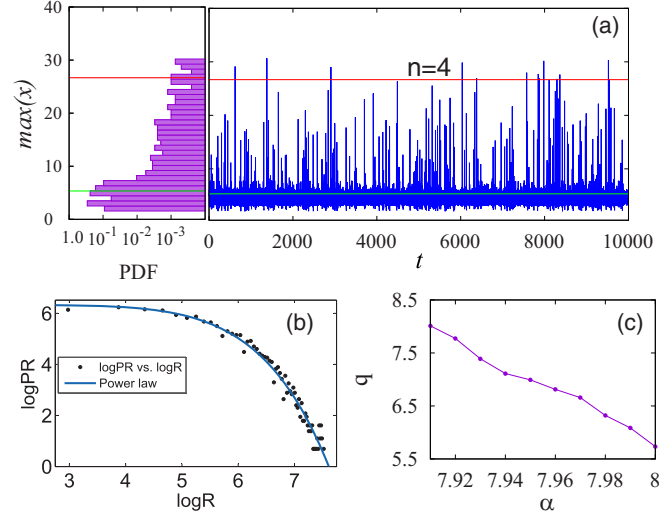


FIG. 4. (a) (Left) Probability distribution function (PDF) and (right) time series of dynamical variable  $x$  for  $\alpha = 7.99$ ,  $\gamma = 0.709$ ,  $\beta = 0.318$ , and  $\omega = 1.28$ . The upper horizontal red line shows the threshold value for extreme events ( $n = 4$ ) and the lower horizontal green line represents average peak amplitude  $\langle x \rangle$ . (b) Probability of recurrence times (PR) exhibiting a power-law behavior (blue curve) with characteristic exponent  $q = 6$  (in log scale with base 10). (c) Scaling exponent of probability distribution of recurrence times versus  $\alpha$ .

panel of Fig. 4(a) we show the time series of the variable  $x$ , where the extreme pulses (above the  $n = 4$  threshold) can clearly be distinguished. In the left panel in the same figure, we plot the corresponding probability distribution function (PDF), which exhibits a long-tailed behavior, typical for extreme events.

The extreme behavior can also be characterized by the probability of recurrence times (PR) versus return intervals ( $R$ ) between subsequent events given as

$$\log_{10}(\text{PR}) = p \log_{10}(R)^q + r, \tag{3}$$

where  $p$  and  $r$  are constants used to fit the data in Fig. 4(b) and  $q$  is the scaling exponent. Our results show that similar to other systems [4,43], the extreme events in MEMS exhibit a power-law probability distribution of the recurrence times (PR). The dependence of the scaling exponent  $q$  on the modulation amplitude  $\alpha$  is shown in Fig. 4(c), when all other parameters are fixed. One can see that  $q$  linearly decreases as  $\alpha$  is increased.

Next, we are interested in how the maximum amplitude  $\max(x_{EE})$  of the extreme events during a relatively long time ( $t = 10000$ ) depends on the modulation amplitude  $\alpha$ . As shown in Fig. 5 by the blue curve, for small  $\alpha$ ,  $\max(x_{EE})$  exhibits an approximately linear growth as  $\alpha$  is increased. Whereas, when  $\alpha$  exceeds a threshold value ( $\alpha > 7.5$ ), the character of this dependency changes,  $\max(x_{EE})$  increases approximately exponentially with  $\alpha$ . At the same time, the average value of the variable  $\langle x \rangle$  remains almost independent of  $\alpha$ , as shown in the same figure by the red lower line.

We also calculated the number of standard deviations over the average value  $\langle x \rangle$  corresponding to  $\max(x_{EE})$  using the

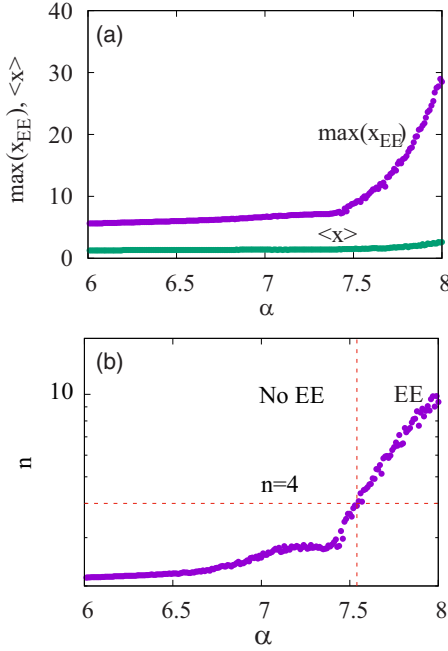


FIG. 5. (a) Maximum amplitude of extreme events  $\max(x_{EE})$  (blue upper line) and average  $x$  (red lower line) as a function of external force amplitude  $\alpha$ . (b) Number of standard deviations above average peak amplitude corresponding to  $\max(x_{EE})$ . The regions without extreme events and with extreme events using  $n = 4$  criterion are marked as “No EE” and “EE,” respectively.

following equation:

$$n_{\max} = \frac{\max(x_{EE}) - \langle x \rangle}{\sigma_x}. \quad (4)$$

The dependency  $n_{\max}(\alpha)$  is shown in Fig. 5(b). One can see that the character of the curve changes when  $\alpha$  exceeds 7.4, where it sharply goes up, thus representing a strong sensitivity to  $\alpha$ .

The extreme events in MEMS appear in a certain range of the modulation amplitude  $\alpha$  and frequency  $\omega$ . In Fig. 6 we plot the diagram of extreme events in the  $(\omega, \alpha)$ -parameter

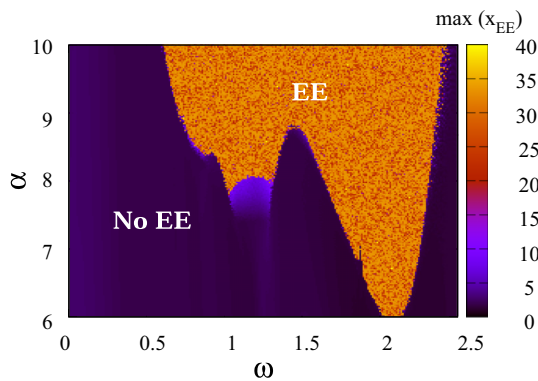


FIG. 6. Two-parameter diagram of extreme event maximum amplitude  $\max(x_{EE})$  in  $(\omega, \alpha)$ -parameter space. Extreme events appear in the orange area marked as EE.

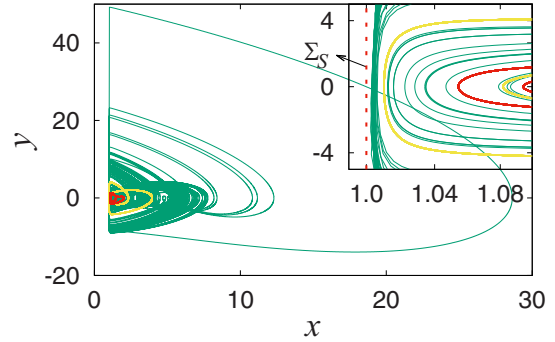


FIG. 7. Phase-space trajectories of modulated MEMS with  $\alpha = 2$  (red),  $\alpha = 4$  (yellow), and  $\alpha = 7.99$  (green). The inset represents zoom close to the discontinuous boundary  $\Sigma_S$  at  $x = 1$  marked by the dashed vertical line. The red and yellow trajectories are far from  $\Sigma_S$  and do not exhibit extreme events. Instead, the green trajectory approaches very close to the discontinuous boundary and then reaches the extreme value.

space. The colors indicate the maximum amplitude  $\max(x_{EE})$  of extreme events. The regions without extreme events (No EE) and with extreme events (EE) are clearly seen in the figure. The tongue structure appears due to a resonance effect when the modulation frequency is close to the natural frequency (around 2) and its subharmonic frequency.

For a better understanding of the mechanisms underlying the emergence of extreme events, in Fig. 7 we plot the phase-space trajectories for three different values of the modulation amplitude: (i)  $\alpha = 2$  (red), (ii)  $\alpha = 4$  (yellow), and (iii)  $\alpha = 7.99$  (green). While the trajectories (i) and (ii) do not display extreme events, the trajectory (iii) does exhibit extreme events. In the inset in Fig. 7, one can see that the trajectories (i) and (ii) are always far away from the discontinuous boundary  $\Sigma_S$  at  $x = 1$ , and therefore they do not exhibit extreme events because the system does not undergo a stick-slip bifurcation. Instead, the trajectory (iii) approaches very close  $\Sigma_S$  that results in sticking and sliding over a long distance and finally repulsing for a long excursion.

#### D. Prediction of extreme events in MEMS

The presence of a large sliding trace along the discontinuous boundary  $\Sigma_S$  allows the extreme event prediction, which can be made by monitoring the phase-space trajectory and time series. As seen from Fig. 7, prior to the extreme event occurrence, the trajectory undergoes a very large sliding motion along  $x \approx 1$ . This behavior can also be distinguished in the time series shown in Fig. 8(a), where a large  $y$  peak amplitude appears before the variable  $x$  begins to increase. Figure 8(b) shows that the extreme events in variable  $x$  occur when the sliding distance  $y_{sd}$  exceeds a critical value  $y_c$ . For a relatively large sliding distance ( $y_{sd} > 20$ ), the peak amplitude  $\max(x)$  is proportional to  $y_{sd}$  and can be approximated by the linear relation  $x_{EE} = 0.4605 y_{sd} - 1.42$  [Fig. 8(c)]. Small peak  $y$  values in the shaded area in Fig. 8(c) correspond to nonsliding trajectories, which are far from the discontinuous boundary. The extreme events in  $x$  can be forecasted with time  $t_f$  before the event reaches its maximum amplitude by

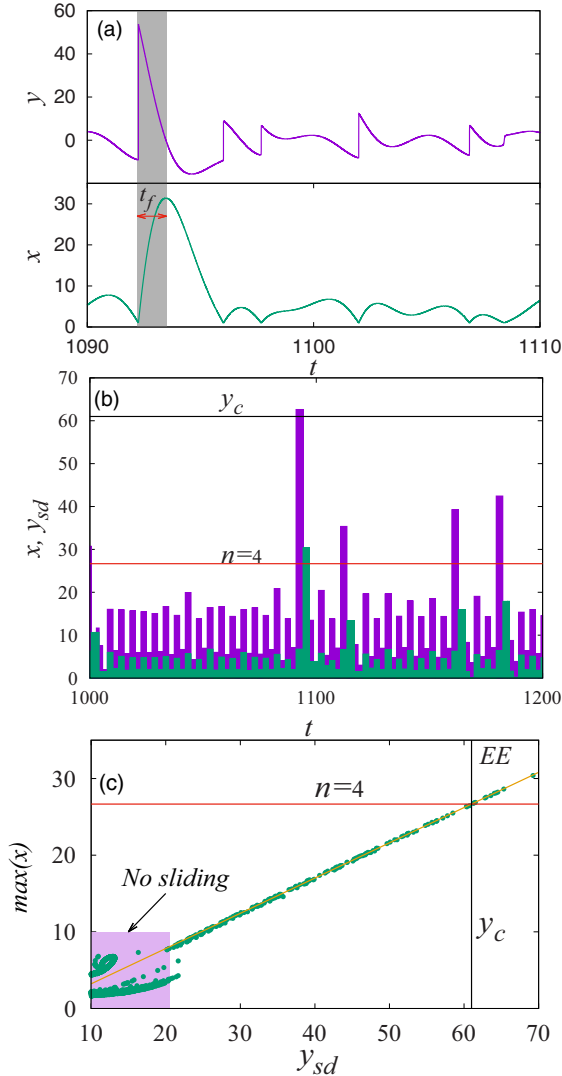


FIG. 8. Extreme event forecasting in MEMS. (a) Time series of variables  $x$  and  $y$ . The variable  $y$  exhibits a long sliding motion before the extreme event occurs in the variable  $x$ . The shaded area shows forecasting time  $t_f$ . (b) Time series of events in  $x$  (green) and sliding distance  $y_{sd}$  (blue). (c) Linear relation between event amplitude  $\max(x)$  and sliding distance  $y_{sd}$  in the sliding regime, and nonlinear in the nonsliding regime (shaded area).

identifying the sliding distance  $y_{sd}$  and its threshold value  $y_c$ . The longer the sliding trace in  $y$ , the higher the extreme event in  $x$  (see Supplemental Movie [41]).

#### IV. SLIDING BIFURCATION AND EXTREME EVENTS IN A CLASS-B LASER

##### A. CO<sub>2</sub> laser model

To demonstrate the generality of this phenomenon, we consider another example of a nonlinear system with a discontinuous boundary, namely a single-mode CO<sub>2</sub> laser modeled by the following equations [31]:

$$\dot{I} = \tau^{-1}(N - k(t))I, \quad \dot{N} = (N_0 - N)\gamma - IN, \quad (5)$$

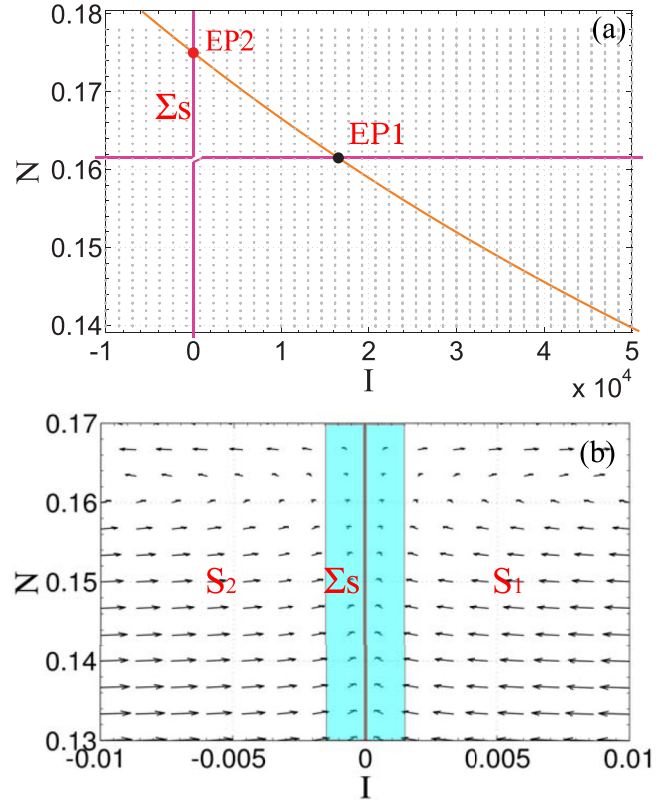


FIG. 9. (a) Nullcline (red line) and equilibrium points EP1 and EP2 (red and black dots) of Eq. (3). (b) Vector field of the CO<sub>2</sub> laser near the discontinuous boundary at  $I = 0$ .

where  $I$  is proportional to the mean radiation density,  $N$  is the laser gain,  $N_0$  is the unsaturated gain of the active medium,  $\gamma$  is the gain decay rate, and  $\tau$  is the half round-trip time of light in the resonator. Here,  $k(t) = k_0(1 + a \cos 2\pi ft)$  is the modulated cavity losses,  $k_0$  is the constant part of the losses, and  $a$  and  $f$  are the driving amplitude and frequency, respectively. In this paper, we use the following constant parameters:  $\gamma = 1.978 \times 10^5 \text{ s}^{-1}$ ,  $\tau = 3.5 \times 10^{-9} \text{ s}$ ,  $N_0 = 0.175$ ,  $k_0 = 0.17$ , and  $f = 208.25 \text{ kHz}$ .

Since the CO<sub>2</sub> laser belongs to class-B lasers, in the absence of external perturbation ( $a = 0$ ) it behaves as a damped oscillator, which trajectory converges to a stable equilibrium point given as  $I_S = \gamma(N_0/k_0 - 1)$  and  $N_S = k_0$ . Another equilibrium point lies on the boundary at  $I_S = 0$  and  $N_S = N_0$ . Figure 9(a) shows the nullclines of the CO<sub>2</sub> laser in the absence of external forcing. It is clearly seen the presence of two equilibrium points, fixed point (EP1) and saddle-node point (EP2). The latter point is situated on the boundary  $I = 0$  and creates a closed discontinuity in the system, imposed by the fact that the intensity cannot be negative ( $I \geq 0$ ).

In Fig. 9(b) we plot the vector field of the CO<sub>2</sub> laser in the absence of external perturbation, i.e., for  $a = 0$ . Since the CO<sub>2</sub> laser displays a sliding set  $\Sigma_S$  near the discontinuous boundary  $I = 0$ , the trajectory stays in the subspace  $S_1$ . Therefore, the driven CO<sub>2</sub> laser is a typical example of a slick-slip system, able to exhibit extreme and super extreme events in the form of large-amplitude oscillations created by a sliding orbit.

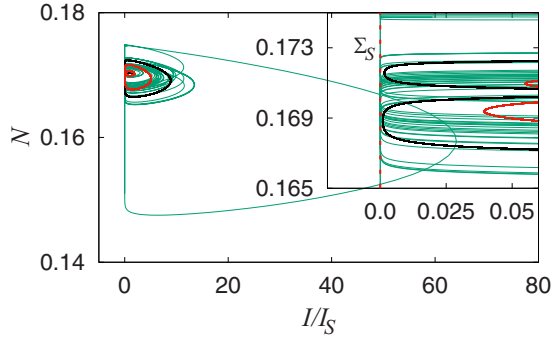


FIG. 10. Phase-space trajectories of the modulated CO<sub>2</sub> laser with amplitudes  $a = 0.05$  (red),  $a = 0.10$  (black), and (iii)  $a = 0.19$  (green). The inset shows zoom close to the discontinuous boundary  $\Sigma_S$  at  $I = 0$  marked by the vertical dashed line.

**B. Extreme event prediction in the CO<sub>2</sub> laser**

Figure 10 shows the phase-space trajectories of the CO<sub>2</sub> laser for three different values of the driving amplitude: (i)  $a = 0.05$  (red), (ii)  $a = 0.10$  (black), and (iii)  $a = 0.19$  (green). Similarly to the MEMS cantilever, the trajectories (i) and (ii) do not exhibit extreme events, whereas the trajectory (iii) shows extreme events. From the inset in Fig. 10, we can see that the trajectories (i) and (ii) are far away from

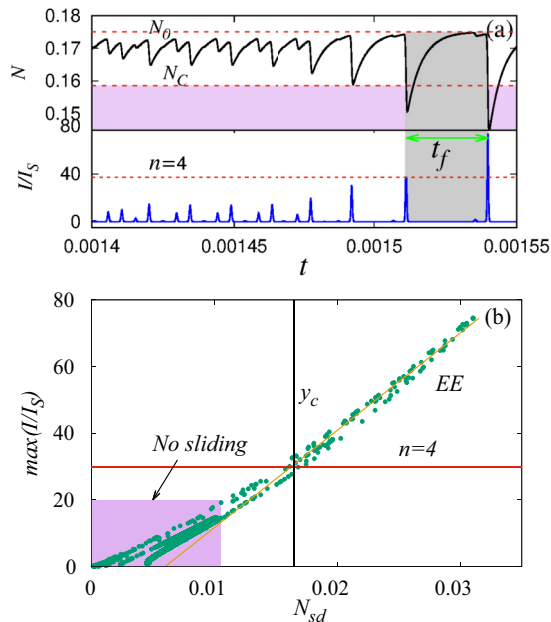


FIG. 11. Extreme event forecasting in the CO<sub>2</sub> laser. (a) Time series of  $N$  and  $I/I_S$  for  $a = 0.19$ . The gray shadow area shows prediction time  $t_f$  for the extreme event. The horizontal dashed lines at  $N_0 = 0.175$ ,  $N_C = 0.158$ , and  $n = 4$  indicate, respectively, the boundary equilibrium point, the threshold gain, and the extreme event criterion. The pulse amplitude is considered to be zero if  $I \leq 10^{-20}$ . (b) Event amplitude  $\max(I/I_S)$  versus sliding distance  $N_{sd}$  exhibits an almost linear relation in the sliding regime and a nonlinear dependence in the nonsliding regime (shaded area). The horizontal and vertical lines indicate the onset of extreme events (EE) defined by the condition  $n = 4$ .

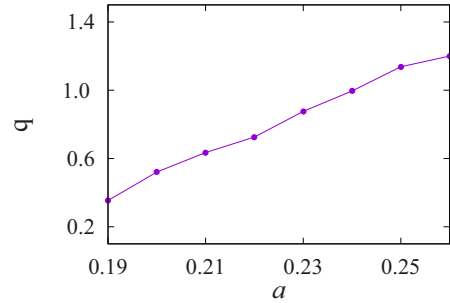


FIG. 12. Characteristic exponent of probability distribution of recurrence time between extreme events in the CO<sub>2</sub> laser as a function of modulation amplitude  $a$ .

the discontinuous boundary  $\Sigma_S$  at  $I = 0$ , and therefore, the system does not undergo a stick-slip bifurcation. Instead, the trajectory (iii) approaches  $\Sigma_S$ , that results in sticking and sliding over a large distance, and makes a long excursion. In the laser, the extreme events are observed close to interior crisis, and the sliding bifurcation occurs just before the crisis point.

The mechanism of extreme events in the CO<sub>2</sub> laser can be better understood by considering the time series of  $N$  and  $I$  shown in Fig. 11(a). Using the same  $n = 4$  criterion as in MEMS, the laser emits extreme intensity pulses after time  $t_f$  when  $N$  crosses the threshold value  $N_C = 0.158$ , where  $N_C$  is defined as  $N_C = N_0 - N_{sd}$  with the critical sliding distance for extreme events being  $N_{sd} = 0.017$ . One can see that before emitting the extreme pulse, the trajectory stays far away from the discontinuous boundary  $I = 0$ , whereas in the regime of extreme events the trajectory approaches closer to  $I = 0$ . At the same time, the variable  $N$  almost reaches the boundary equilibrium point  $N_0 = 0.175$ .

The extreme events in the CO<sub>2</sub> laser also obey a linear dependence of the maximum amplitude  $I/I_S$  on  $N_{sd}$ , i.e.,  $I_{EE} = 2.9 \times 10^3 N_{sd} - 17.32$ , as shown in Fig. 11(b).

Similar to the MEMS cantilever, the emergence of extreme events in the CO<sub>2</sub> laser can be predicted by monitoring one of the variables, in particular, by measuring the sliding distance  $N_{sd}$ . Practically, this can be done using the experimental technique proposed in Ref. [30].

The probability distribution of recurrence time in the CO<sub>2</sub> laser also obeys a power law. However, in contrast to MEMS, the scaling exponent grows as the modulation amplitude is increased. This dependence is shown in Fig. 12, when other laser parameters remain fixed. One can see that  $q$  grows approximately linearly as  $a$  is increased.

**V. CONCLUSION**

To conclude, we have introduced a new class of extreme events which appear in dissipative dynamical systems with discontinuous boundaries. These systems exhibit extreme events when the trajectory approaches very close to the discontinuous boundary due to the existence of both a sliding set and a stick-slip bifurcation. The amplitude of the extreme event is related to the sliding distance of the trajectory along the discontinuous boundary and obeys a power-law probability distribution of recurrence time. Early warning signals of this kind of extreme events can be detected by monitoring

the phase-space trajectory or directly from time series of the sliding variable. The longer the sliding distance, the stronger the extreme event.

As examples of such systems, we have considered a MEMS cantilever and a loss-modulated CO<sub>2</sub> laser. In both cases, the probability distribution of recurrence time displays a power-law scaling behavior, typical of extreme events. We have shown that the emergence of extreme events in both cases can be predicted by measuring the sliding distance of one of the variables.

We believe that the results of this work are not only of fundamental interest but can also be useful in engineering

applications for characterization and prediction of extreme events in systems with discontinuous boundaries, such as cantilevers, systems with friction, lasers, etc.

#### ACKNOWLEDGMENTS

S.K. acknowledges support from the Technical University of Madrid and a Dr. D. S. Kothari Postdoctoral Fellowship from the University Grants Commission (India). A.N.P. thanks to the Ministry of Economy and Competitiveness (Spain) (Project No. SAF2016-80240) for financial support.

- 
- [1] S. Albeverio, V. Jentsch, and H. Kantz, *Extreme Events in Nature and Society* (Springer, Berlin, 2006).
- [2] C. Nicolis, V. Balakrishnan, and G. Nicolis, *Phys. Rev. Lett.* **97**, 210602 (2006).
- [3] G. Nicolis and C. Nicolis, *Foundations of Complex Systems*, 2nd ed. (World Scientific, Singapore, 2012).
- [4] P. Bak, K. Christensen, L. Danon, and T. Scanlon, *Phys. Rev. Lett.* **88**, 178501 (2002).
- [5] A. N. Ganshin, V. B. Efimov, G. V. Kolmakov, L. P. Mezhov-Deglin, and P. V. E. McClintock, *Phys. Rev. Lett.* **101**, 065303 (2008).
- [6] A. Mussot, A. Kudlinski, M. Kolobov, E. Louvergneaux, M. Douay, and M. Taki, *Opt. Express* **17**, 17010 (2009).
- [7] H. Bailung, S. K. Sharma, and Y. Nakamura, *Phys. Rev. Lett.* **107**, 255005 (2011).
- [8] R. Höhmann, U. Kuhl, H.-J. Stöckmann, L. Kaplan, and E. J. Heller, *Phys. Rev. Lett.* **104**, 093901 (2010).
- [9] J. J. Metzger, R. Fleischmann, and T. Geisel, *Phys. Rev. Lett.* **112**, 203903 (2014); A. Mathis, L. Froehly, S. Toenger, F. Dias, G. Genty, and J. M. Dudley, *Sci. Rep.* **5**, 12822 (2015); S. Birkholz, C. Brée, I. Veselić, A. Demirçan, and G. Steinmeyer, *ibid.* **6**, 35207 (2016).
- [10] F. T. Arecchi, U. Bortolozzo, A. Montina, and S. Residori, *Phys. Rev. Lett.* **106**, 153901 (2011).
- [11] C. Kharif and E. Pelinovsky, *Eur. J. Mech. B* **22**, 603 (2003).
- [12] P. K. Shukla, I. Kourakis, B. Eliasson, M. Marklund, and L. Stenflo, *Phys. Rev. Lett.* **97**, 094501 (2006).
- [13] F. Baronio, M. Conforti, A. Degasperis, S. Lombardo, M. Onorato, and S. Wabnitz, *Phys. Rev. Lett.* **113**, 034101 (2014).
- [14] B. Kibler, A. Chabchoub, A. Gelash, N. Akhmediev, and V. E. Zakharov, *Phys. Rev. X* **5**, 041026 (2015).
- [15] D. R. Solli, C. Ropers, P. Koonath, and B. Jalali, *Nature (London)* **450**, 1054 (2007).
- [16] A. N. Pisarchik, R. Jaimes-Reátegui, R. Sevilla-Escoboza, G. Huerta-Cuellar, and M. Taki, *Phys. Rev. Lett.* **107**, 274101 (2011).
- [17] J. Zamora-Munt, B. Garbin, S. Barland, M. Giudici, Jose R. Rios Leite, C. Masoller, and J. R. Tredicce, *Phys. Rev. A* **87**, 035802 (2013).
- [18] H. L. D. de S. Cavalcante, M. Oriá, D. Sornette, E. Ott, and D. J. Gauthier, *Phys. Rev. Lett.* **111**, 198701 (2013).
- [19] S. L. Kingston, K. Thamilaran, P. Pal, U. Feudel, and S. K. Dana, *Phys. Rev. E* **96**, 052204 (2017).
- [20] C. Bonatto, M. Feyereisen, S. Barland, M. Giudici, C. Masoller, J. R. Rios Leite, and J. R. Tredicce, *Phys. Rev. Lett.* **107**, 053901 (2011); M. G. Kovalsky, A. A. Hnilo, and J. R. Tredicce, *Opt. Lett.* **36**, 4449 (2011).
- [21] M. Onorato, T. Waseda, A. Toffoli, L. Cavaleri, O. Gramstad, P. A. E. M. Janssen *et al.*, *Phys. Rev. Lett.* **102**, 114502 (2009); M. Shats, H. Punzmann, and H. Xia, *ibid.* **104**, 104503 (2010).
- [22] A. Toffoli, D. Proment, H. Salman, J. Monbaliu, F. Frascoli, M. Dafilis, E. Stramignoni, R. Forza, M. Manfrin, and M. Onorato, *Phys. Rev. Lett.* **118**, 144503 (2017).
- [23] C. L. E. Franzke, *Chaos* **27**, 012101 (2017).
- [24] C. Bonatto and A. Endler, *Phys. Rev. E* **96**, 012216 (2017).
- [25] V. Odent, M. Taki, and E. Louvergneaux, *Nat. Hazards Earth Syst. Sci.* **10**, 2727 (2010); A. Karsaklian dal Bosco, D. Wolfersberger, and M. Sciamanna, *Opt. Lett.* **38**, 703 (2013).
- [26] C. Metayer, A. Serres, E. J. Rosero, W. A. S. Barbosa, F. M. de Aguiar, J. R. Rios Leite, and J. R. Tredicce, *Opt. Express* **22**, 19850 (2014); N. M. Granese, A. Lacapmesure, M. B. Agüero, M. G. Kovalsky, A. A. Hnilo, and J. R. Tredicce, *Opt. Lett.* **41**, 3010 (2016).
- [27] E. J. Gumbel, *Statistics of Extremes* (Dover, New York, 2004).
- [28] N. Hoffmann and L. Gaul, *J. Appl. Math. Meth.* **83**, 524 (2003); M. Guardia, S. J. Hogan, and T. M. Seara, *SIAM J. Appl. Dyn. Syst.* **9**, 769 (2010); P. M. Geffert and W. Just, *Phys. Rev. E* **95**, 062111 (2017).
- [29] S. Liu, A. Davidson, and Q. Lin, *J. Micromech. Microeng.* **14**, 1064 (2004); D. R. Evans, P. Tayati, H. An, P. K. Lam, V. S. J. Craig, and T. J. Senden, *Sci. Rep.* **4**, 5567 (2014).
- [30] A. N. Pisarchik, *Opt. Quantum Electron.* **20**, 313 (1988).
- [31] V. N. Chizhevsky, R. Corbalán, and A. N. Pisarchik, *Phys. Rev. E* **56**, 1580 (1997).
- [32] C. Kuehn and P. Szmolyan, *J. Nonlinear Sci.* **25**, 583 (2015).
- [33] L. Li and A. C. Luo, *Int. J. Bifurcation Chaos* **26**, 1650224 (2016).
- [34] A. F. Filippov, *Differential Equations with Discontinuous Right-hand Sides* (Springer, London, 1988).
- [35] R. I. Leine, D. H. Van Campen, and B. L. Van de Vrande, *Nonlin. Dyn.* **23**, 105 (2000).
- [36] M. Bernardo, P. Kowalczyk, and A. Nordmark, *Physica D (Amsterdam)* **170**, 175 (2002).
- [37] Y. A. Kuznetsov, S. Rinaldi, and A. Gagnani, *Int. J. Bifurcation Chaos* **13**, 2157 (2003).

- [38] M. di Bernardo, C. J. Budd, A. R. Champneys, and P. Kowalczyk, *Piecewise-Smooth Dynamical Systems: Theory and Applications* (Springer, London, 2008).
- [39] W. F. Brace and J. D. Byerlee, *Science* **153**, 990 (1966).
- [40] H. J. S. Feder and J. Feder, *Phys. Rev. Lett.* **66**, 2669 (1991).
- [41] See Supplemental Material at <http://link.aps.org/supplemental/10.1103/PhysRevE.98.032203> for a movie.
- [42] V. Choudhary and K. Iniewski (eds.), *MEMS: Fundamental Technology and Applications* (CRC Press, New York, 2013).
- [43] E. G. Altmann and H. Kantz, *Phys. Rev. E* **71**, 056106 (2005); M. S. Santhanam and H. Kantz, *ibid.* **78**, 051113 (2008).